Radiation damage to a protein solution, detected by synchrotron X-ray small-angle scattering: dose-related considerations and suppression by cryoprotectants

Shigeo Kuwamoto, Shuji Akiyama and Tetsuro Fujisawa*

Laboratory for Structural Biochemistry, RIKEN Harima Institute/SPring-8, 1-1-1 Kouto, Mikazuki, Sayo, Hyogo 679-5148, Japan. E-mail: fujisawa@spring8.or.jp

In small-angle X-ray scattering experiments at high-brilliant synchrotron sources, protein aggregation results from radiation damage. The radiation-induced aggregation of lysozyme in solution was qualitatively evaluated based on forward scattering and radii of gyration. The scattering did not change below 400 Gy and increased exponentially above this dose. The aggregation is only seen beyond the critical dose rate, and the 'dilution effect' known in radiology was also observed. Mass spectroscopy of the lysozyme solution exposed to a monochromatic X-ray beam did not show any cleavage of the polypeptide chain. Small-angle X-ray scattering patterns suggested that the radiation-induced aggregation should be a non-specific association of intact lysozyme, without substantial alterations of the folding topologies. It was found that the addition of small amounts of cryoprotectants, such as glycerol, ethylene glycol and sucrose, effectively reduced the radiation damage. Glycerol and ethylene glycol were identically effective in the 100 m*M* concentration range. A similar effective concentration was observed for sucrose. The damage reduction by the cryoprotectants was mainly ascribed to changes in the protein–protein interactions, and rarely to decreases in the diffusion rates of activated species.

Keywords: radiation damage; synchrotron X-ray small-angle scattering; glycerol; ethylene glycol; sucrose.

1. Introduction

Radiation damage to biomacromolecules has become a serious problem in modern structural biology since intense X-ray beams became available at third-generation X-ray sources. In the field of protein crystallography, the damage is often seen in both real and reciprocal space, as in the increased mosaicity of the crystal, $R_{\rm sym}$, and Wilson *B* factors and the disruption of intramolecular disulfide bridges seen in the electron density map (O'Neill *et al.*, 2002; Murray & Garman, 2002; Teng & Moffat, 2000, 2002). The situation is much worse in protein solutions at room temperatures without the cryo-cooling technique. The physicochemical properties of radiation damage to protein solutions have been studied extensively in the field of radiology, where solutions were irradiated with 10^{14}–10^{15} photons s^{-1} of white X-rays in 5–30 keV (Garrison, 1987; Maleknia *et al.*, 2001). The reaction of the incident X-ray with water molecules creates hydroxyl or hydroperoxyl radicals that rapidly attach to the backbones and/or side chains of proteins (10^9–10^{10} M^{-1} s^{-1}). In many cases the interactions between the radical-activated proteins give rise to radiation-induced aggregates connected to each other by covalent and/or non-covalent bonds (Garrison, 1987).

Synchrotron X-ray small-angle scattering (SXSS) measurements at undulator beamlines typically use a monochromatic X-ray beam ranging from 5×10^{10} to 5×10^{13} photons s^{-1} at 8–14 keV, with a submillimeter square size. The exposure time varies from subsecond to several hundred seconds depending on the experimental purposes. In SXSS experiments the radiation appears most conspicuously as radiation-induced aggregations. The accumulation of the aggregates mostly interferes with the small-angle region, where the size and shape information of the target proteins resides. Although the spatial resolution of SXSS is usually lower than that of protein crystallography, a recent study pointed out that not only the small-angle but also the high-resolution wide-angle X-ray scattering could be modulated by the growth of radiation-induced aggregates (Fischetti *et al.*, 2003). Therefore, reduction of the radiation damage is indispensable for correct interpretations as well as quantitative analyses. The use of a flow cell has been practically successful for reducing radiation damage (Fischetti *et al.*, 2003). However, little has been reported about the dose-related considerations of radiation-induced aggregation in solutions at moderate temperatures.

Radiologists have pointed out that reducing agents, such as ethanol, Tris, EDTA and DTT, serve as radical scavengers for reducing the radiation damage of proteins (Maleknia *et al.*, 2001). Recently, protein crystallographers found that high concentrations of the cryoprotectants, such as glycerol, ethylene glycol, PEG, glucose and other sugars, could effectively reduce the radiation damage to protein crystals (O'Neill *et al.*, 2002). However, care must be exercised when using these agents since high concentrations of cryoprotectants could have a variety of side effects on the protein solutions, such as modulations of protein stabilities, decreases in protein volumes, increases in solvent viscosities and reductions of scattering contrasts.

In order to seek out approaches to reduce radiation damage in SXSS measurements, we have investigated the monochromatic radiation-induced aggregation of hen egg-white lysozyme, which is a monomeric protein containing four intrachain disulfide bonds (14.3 kDa). This paper consists of two parts: the quantitative evaluation and understanding of the dose-related phenomena of radiation-induced aggregation, and a preliminary study on the scavenging effects of the cryoprotectants.

2. Materials and methods

2.1. Sample preparations

Hen egg-white lysozyme was purchased from Sigma (L6876, recrystallized three times). All other chemicals of the highest grade available were purchased from Wako Pure Chemical Industries. The lysozyme was dissolved in 40 m*M* sodium acetate at pH 3.8, containing 150 m*M* NaCl, and was filtered with a 0.22 µm membrane filter. The monodispersity of the lysozyme solution was checked by dynamic light scattering (DynaPro, Protein Solutions). The diffusion coefficient of lysozyme was $\sim 1.08 \times 10^{-6} \pm 0.02 \times 10^{-6}$ cm^2 s^{-1}, or 19.1 ± 1.5 Å of the Stokes radius at 293 K. The concentration of lysozyme was determined using the absorption coefficient, $A_{280}^{1\,{\rm mg\,ml^{-1}}} = 2.64$. Since the concentrations of the cryoprotectants were low, their dilutions from the mother liquor were carefully performed, in order to ensure their accuracy. The concentrations of the cryoprotectants were estimated by the reflectivity (*Handbook of Chemistry and Physics*, Boca Raton, Florida: CRC Press). The radiation-induced cleavage of lysozyme was monitored by comparing the SDS-PAGE profiles before and after the irradiation. In order to enhance the SDS-PAGE resolution, a tricine buffer system was used instead of the standard glycine buffer (Schagger & von Jagow, 1987). The acrylamide concentration was 16.5%. More detailed evaluations were performed with mass spectroscopy (TOF-mass) experiments using Voyager-DE Pro (Applied Biosystems).

  doi:10.1107/S0909049504019272

2.2. SXSS measurements

SXSS measurements were carried out using the RIKEN structural biology beamline I (BL45XU) (Fujisawa *et al.*, 2000), which employs a 0.9 Å X-ray wavelength from an undulator source of the electron storage ring at SPring-8 (Harima, Japan). The wavelength width, $\Delta\lambda/\lambda$, is below 10^{-4}. The photon flux, n, was estimated according to the following equation,

$$n = (W/Ee)\{I/[1 - \exp(-\mu l)]\}, \quad (1)$$

where I is the ion chamber current, W is the average lost energy of incident photons per generated ion pair, E is the photon energy, e is the electron charge, μ is the linear absorption coefficient of air, and l is the length of the electrode. The incident flux at the sample position was estimated to be 1–2 $\times$ 10^{11} photons s^{-1}. The linear absorption coefficient was interpolated with the values for dry air near sea level reported by ICRU (ICRU, 1989). The absorbed energy, D (Gy), *i.e.* the accumulated dose, was estimated using the following equation,

$$D = (\mu/\rho)nteE/A, \quad (2)$$

where μ/ρ is the absorption coefficient of water, n is the photons per second, t is the radiation time, and A is the radiation area at the sample point. The beam size at the sample cell was determined to be 800 µm (horizontal) $\times$ 600 µm (vertical) by a slit scan. The path length of the sample cuvette was 3 mm, and the window material was synthetic quartz of thickness 20 µm. The temperature of 50 µl of the sample in the cuvette was controlled by a pelche-based cell holder (HE-11259, Teikoku Electronic MFG, Japan), which employs a thin-film thermosensor together with a dynamic thermocontrol algorithm in order to realise rapid temperature changes (10 K min^{-1}) with high precision ($\pm$0.1 K).

The samples were irradiated continuously with X-rays, and the scattering profiles were collected with a detector consisting of an X-ray image intensifier equipped with a cooled CCD (XR-II + CCD) (Fujisawa *et al.*, 1999), which allows continuous data acquisition with a time frame of 0.5–1 s. We measured three data sets in order to ensure the reproducibility. The sample-to-detector distance was 660 mm, calibrated by the meridional reflections from chicken collagen. Preliminary data processing was performed using the program *iisgnapr*, as previously described (Fujisawa *et al.*, 2001). The reciprocal parameter, S, is equal to $2\sin\theta/\lambda$ (where 2θ is the scattering angle and λ is the X-ray wavelength). The radius of gyration, R_g, was determined by fitting the intensity profiles under the Guinier approximation (Guinier & Fournet, 1955),

$$I(S) = I(0)\exp(-4\pi^2 R_g^2 S^2/3), \quad (3)$$

where $I(0)$ is the forward-scattering intensity at a zero angle. The fitting region used was from 25 $\times$ 10^{-6} $Å^{-2}$ to 45 $\times$ 10^{-6} $Å^{-2}$ in S^2. The protein concentration was 4.9–5.2 mg ml^{-1}. The smoothness of the surface of the scatterers was assessed by a power law analysis (Zarzycki, 1987),

$$I(S) \propto S^{-F_D}. \quad (4)$$

In the case of a smooth surface, F_D approaches 4, according to Porod's law (Guinier & Fournet, 1955). In the case of a random coil, *i.e.* an unfolded protein, F_D decreases to 2, theoretically.

3. Results and discussion

3.1. General aspects of radiation damage seen in SXSS

3.1.1. No cleavage of polypeptide chains by monochromatic irradiation. Protein polypeptide chains are often cleaved by irradiation with white X-rays (5–30 keV, 10^{14}–10^{15} photons s^{-1}). This phenomenon is preferably utilized in footprinting experiments to identify the structures of macromolecular folding intermediates (Maleknia *et al.*, 2001). We first checked for the potential cleavage of lysozyme by monochromatic irradiation under the standard SXSS data-collection conditions. Fig. 1(*a*) illustrates the SDS-PAGE analysis of lysozyme just before and after the irradiation. Both the intensity and pattern of the lysozyme band remained unchanged with up to 8700 Gy of accumulated doses. This result clearly indicates that substantial cleavage, such as that observed for white radiation (Garrison, 1987; Maleknia *et al.*, 2001), does not occur under our experimental conditions.

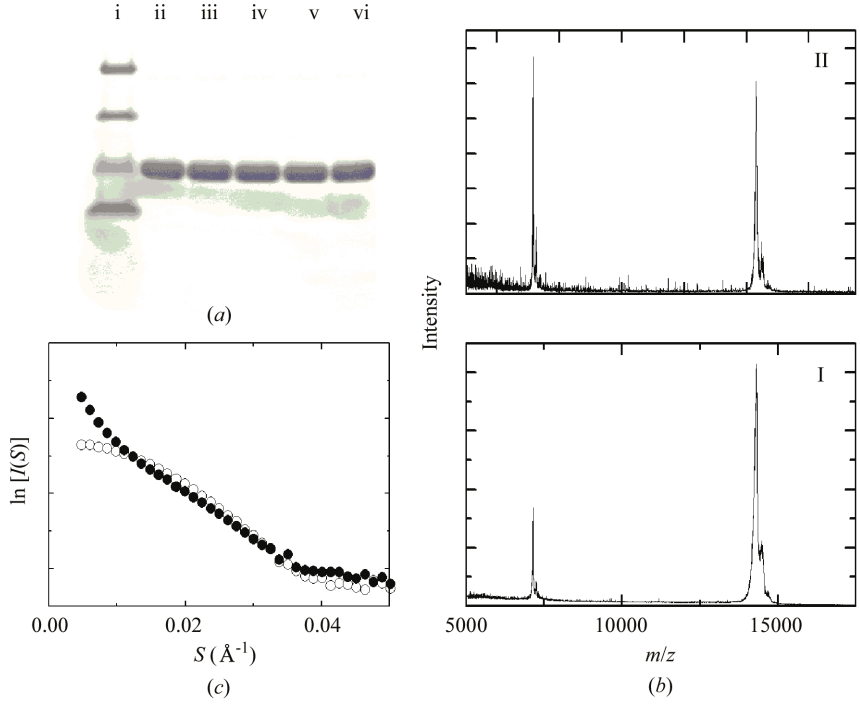

Figure 1
Chemical check for the polypeptide cleavage of lysozyme by monochromatic irradiation. (*a*) SDS polyacrylamide gel analysis of lysozyme solutions with different levels of accumulated doses. (i) Molecular weight markers are: triosephosphate isomerase (26.6 kDa), myoglobin (16.9 kDa), α-lactoalbumin (14.4 kDa) and aprotinin (6.5 kDa); (ii) no exposure; (iii) 433 Gy (144 Gy s^{-1}); (iv) 1406 Gy (141 Gy s^{-1}); (v) 4359 Gy (145 Gy s^{-1}); (vi) 8700 Gy (145 Gy s^{-1}). The lysozyme concentration used in the SXSS measurements was 5 mg ml^{-1}. (*b*) TOF-mass spectra of lysozyme (I) before and (II) after irradiation with 8700 Gy (145 Gy s^{-1}). The matrix buffer was sinapic acid. (*c*) An example of the change in SXSS of lysozyme before and after the monochromatic irradiation. Open circles represents short-exposure lysozyme (165 Gy) while solid circles express long-exposure lysozyme (3300 Gy). An upward curvature in the small S region (solid circles) points to the presence of radiation-induced aggregates. The protein concentration was 4.9 mg ml^{-1}.

According to a previous study (Maleknia *et al.*, 2001), the reactivity order of side chains by synchrotron radiolysis is Cys, Met >> Phe, Tyr > Trp > Pro > His, Leu. A highly solvent accessible environment is more susceptible to OH radicals (Maleknia *et al.*, 2001). The oxidizable sites of lysozyme are Trp62 and Trp123, which are located near the surface (Smith *et al.*, 1993). The molecular weights of the peptides expected from cleavages at these two points are 717, 6613, 7019, 7312 and 13614 Da. The SDS-PAGE results alone do not rule out these potential cleavages completely, owing to the lower sensitivity with smaller peptides (Fig. 1*a*). We therefore performed a more detailed analysis by measuring the TOF-mass spectra before and after irradiation. After irradiation the lysozyme sample is more difficult to ionize so that its TOF-mass spectra became more noisier [see part II of Fig. 1(*b*)]. As shown in Fig. 1(*b*), the exposure to 8700 Gy did not affect the essential features of the TOF-mass spectra, in which only two mass peaks of intact lysozyme were observed (Z = 1 and 2). We therefore conclude that the monochromatic radiation-induced cleavages of the polypeptide chains are negligibly small, if any.

3.1.2. Dose efffects. Continuous irradiation of the lysozyme solution with an intense monochromatic X-ray led to the accumulation of aggregated species. As shown in the inset of Fig. 2, both $I(0)$ and R_g^2 increased with the irradiation time, *i.e.* the absorbed energy increased. To calculate the increase in the ratios of R_g^2 and $I(0)$ we will define the following,

$$F_{RG} = (R_g^2)_D/(R_g^2)_0, \tag{5}$$

$$F_{I0} = \frac{[I(0)]_D}{[I(0)]_0} = \frac{\sum_m N_m I_m(0)}{I_1(0)\sum_m mN_m} = \frac{\sum_m m^2 N_m}{\sum_m mN_m}, \tag{6}$$

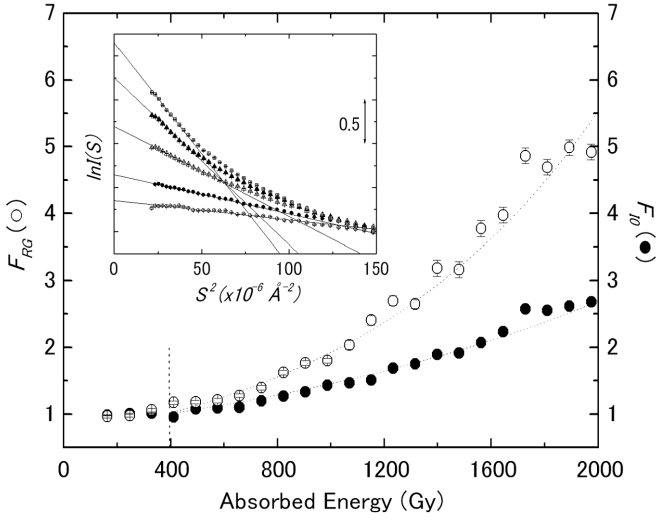

Figure 2
Dependence of R_g and $I(0)$ on the accumulated dose. The lysozyme solution (4.9 mg ml^{-1}) was continuously irradiated by the monochromatic X-ray, and the scattering profiles were recorded with a constant time resolution of 0.53 s. The incident flux and dose rate were 2.2 × 10^{11} photons s^{-1} and 155 Gy s^{-1}, respectively. The increases in R_g and $I(0)$ were expressed as F_{RG} (open circles) and F_{I0} (solid circles), respectively. These definitions are given in equations (5) and (6) (see text). Above 400 Gy, both F_{RG} and F_{I0} followed exponential increases, as formulated in equation (7) (broken lines). The inset represents the Guinier plots at different exposure times, *i.e.* the absorbed energy. The profiles from the bottom to the top correspond to 165, 820, 1645, 2470 and 3300 Gy. The lines show the least-square fitting on the S^2 range, from 20 × 10^{-6} to 45 × 10^{-6} Å^{-2}, obtained by using equation (3).

where the subscript D denotes the value of the accumulated doses, and N_m is the molar number of *m-mer* of lysozyme. Since $I(0)$ of *m-mer* lysozyme is proportional to the square of m, the increases in F_{I0} indicate the occurrence of radiation-induced aggregation. It is worth mentioning the difference between F_{I0} and the survival rate, which is often used in radiology. As is obvious from equation (6), F_{I0} is not simply proportional to the number of intact molecules (N_1).

As shown in Fig. 2, both F_{RG} and F_{I0} basically increased with exposure time, *i.e.* the absorbed energy. However, our detailed examination of the overall data revealed that the accumulation of radiation damage is not a monotonous process. A threshold of radiation insensitivity was observed below 400 Gy, where no radiation-induced aggregation was detected. We call this offset dose the 'critical dose' hereafter. Above the critical dose of 400 Gy, the aggregation processes can be approximated by an exponential function,

$$Y = \exp\big[k_{app}(X - 400)\big], \tag{7}$$

where Y is either F_{RG} or F_{I0}, X is the absorbed energy and k_{app} is the apparent rate of the aggregation (Gy^{-1}). The absorbed energy D is proportional to the time t [see equation (2)], and k_{app} is inversely proportional to t, like a standard rate constant. This critical dose is observed not only for lysozyme but also for other proteins that were measured at our beamline (data not shown). What is the origin of the critical dose? One possible explanation is that radiation-induced aggregation occurs only when at least two proteins or 'targets' are activated. The classical theory of a 'dose effect curve', *e.g.* a 'survival curve' for a single target, is represented by $\exp(-\upsilon D)$, where υ is a radiation-sensitive parameter. In this case, the radiation damage follows exponentially, even with a small exposure dose. In the case where the damage is only seen when two or more multiple (m) targets are necessary, the dose effect curve is written as $1 - [1 - \exp(-\upsilon D)]^m$, which suggests the existence of a threshold in small D (Zimmer, 1961). Consequently, a similar argument would apply for F_{I0}.

Our SXSS data rule out the radiation-induced unfolding of lysozyme, while the disulfide bond breakage at Cys6–Cys127 was observed in the crystalline state (Weik *et al.*, 2000). Even if it was unfolded, the heat-denatured lysozyme under these solvent conditions, *i.e.* acidic pH, did not aggregate even at high protein concentrations (Arai & Hirai, 1999). Fig. 3 illustrates the macroscale surface fractal, which reflects the large-scale surface defects of proteins and is sensitive to the compactness (Zarzycki, 1987; Timchenko *et al.*, 1997). In the region from 0.016 to 0.028 Å^{-1} in S, the surface fractal dimensions determined from the tangents of the fitted lines were well conserved (2.6–2.8) irrespective of the amount of aggregation (Fig. 3). This result suggests that the radiation-induced aggregation of lysozyme is not accompanied by the unfolding of the polypeptide. In other words, the aggregation occurs as a result of the association among the damaged proteins, rather than the association of the unfolded proteins.

3.1.3. Protein concentration effects. Radiation effects in solution apparently depend on the protein concentration (Butler *et al.*, 1960), and our results also showed this behavior. As shown in Fig. 4(*a*), the dose-dependent increases in F_{I0} were dramatically enhanced at the lower protein concentrations. This effect is known as the 'dilution effect': the radiation damage will double by a twofold dilution (Butler *et al.*, 1960). Consistently, as shown in Fig. 4(*b*), the apparent rate of aggregation (k_{app}) was proportional to the protein concentration (2–22 mg ml^{-1}). However, the rate constants normalized relative to the protein concentration were nearly constant (k_{norm} =

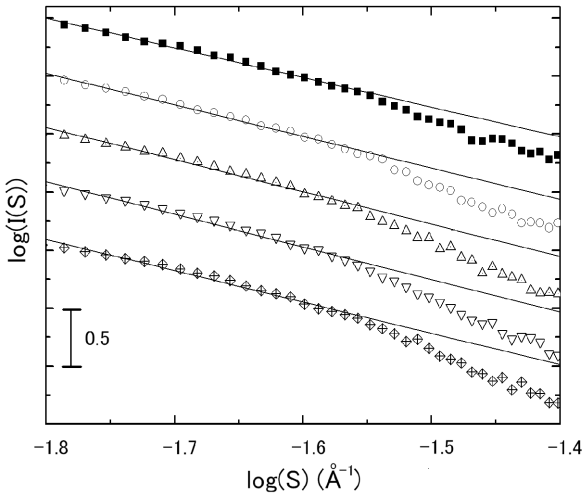

Figure 3
Power-law behaviors of the SXSS profiles of lysozyme. Experimental conditions were the same as in Fig. 2. The scattering curves from the top to bottom correspond to 165, 820, 1645, 2470 and 3300 Gy. Each profile is offset for clarity of presentation.

$k_{app}C$ mg ml^{-1} Gy^{-1}) over 10 mg ml^{-1}, indicating that the dose necessary for radiation-induced aggregation per molecule is independent of C. This result clearly demonstrates that a constant amount of OH radical, created by a unit dose, activates a certain amount of protein molecules.

3.1.4. Dose rate effects. The results described in the previous sections demonstrate that the aggregation-induced radiation damage is free-radical mediated. At the higher flux density, the difference between the rate of radical generation and that of radical loss is so small that recombination reactions are expected. In a lipid membrane system, Cherezov *et al.* (2002) reported two opposite modes of dose-rate effects: type I damage, which broadens the higher-order lamellar reflections and reduces the intensity, showed an 'inverse dose effect', *i.e.* the degradation is more pronounced at a weaker dose rate; type II damage, which has neither line broadening nor the development of diffuse scattering, showed the opposite effect (Cherezov *et al.*, 2002).

Fig. 5 shows that the development of the aggregation increased as the dose rate increased, which was the same as the type II damage in the lipid system. Interestingly, the type II damage also showed a threshold of radiation damage (Cherezov *et al.*, 2002), like Fig. 2. Cherezov *et al.* (2002) also suggested that the different dispersion

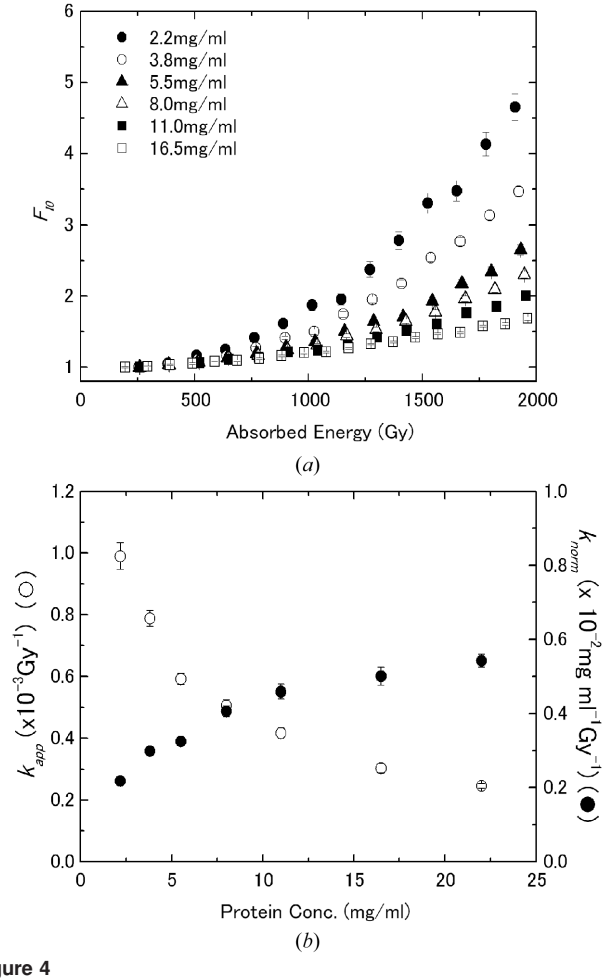

Figure 4
Effects of the protein concentration on the radiation-induced aggregation. (*a*) Increase in $I(0)$ with absorbed energy. The protein concentration of each symbol is shown. It is obvious that the aggregation becomes more conspicuous as the protein concentration decreases. (*b*) Concentration dependence of the aggregation time constants, defined by the exponential function in equation (7). The left-hand axis shows k_{app} and the right-hand axis and solid circles show k_{norm}. The dose rate was 165 Gy s^{-1}.

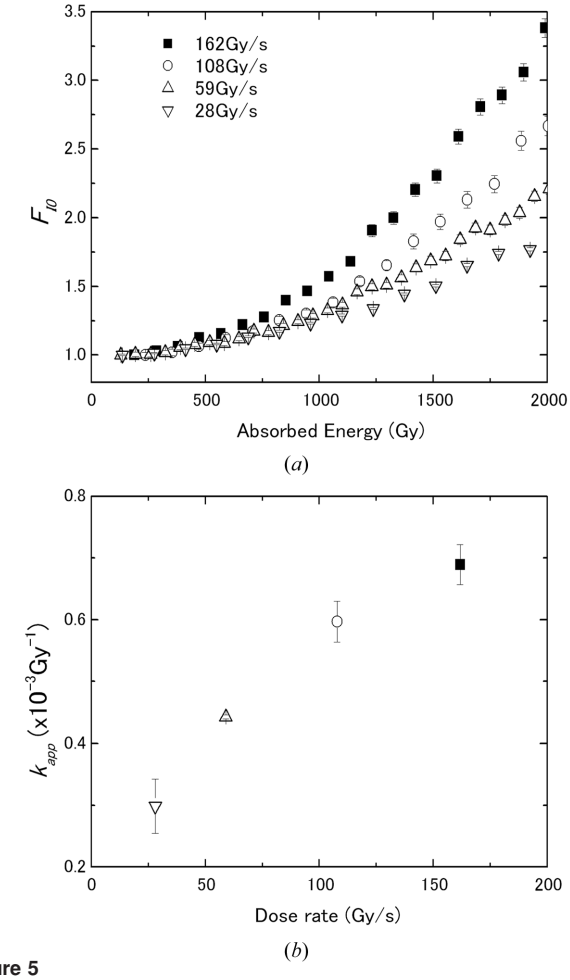

Figure 5
Dependence of the radiation-induced aggregation on the dose rates at 293 K. Inserting aluminium plates changed the dose rates. The lysozyme concentration was 5.2 mg ml^{-1}. (*a*) Radiation-induced aggregation as a function of the dose rate. Below 10 Gy s^{-1}, no appreciable increases in $I(0)$ were observed. (*b*) The apparent rate of the aggregation, determined by fitting to the exponential function in equation (7). In the dose rate below 10 Gy s^{-1}, there was no apparent dependence.

conditions between the damage types I and II can be ascribed to the opposite dose rate effects. Like the type II condition, a protein solution is highly mobile and the radical products can easily diffuse away from the site of their production. At a higher dose rate, the radical-activated lysozyme will be more concentrated and associated for a given dose.

3.1.5. Temperature effects on radiation-induced aggregation. To address the nature of the aggregation processes, we investigated the dependence of the rate constants on the temperature from 278 to 313 K. As shown in Fig. 6, the aggregation rate constant slightly increased with temperature; however, a very small temperature dependence of the radiation damage was observed. The present temperature independency clearly excludes the large conformational change of lysozyme in the radiation-induced aggregation process, which consequently accompanies large temperature dependency, *i.e.* activation energy. This is also consistent with the structural result shown in Fig. 3. The interpretation of this temperature independency is, however, still controversial because reactions of water radicals are generally varied.

3.2. Effects of cryoprotectants on radiation-induced aggregation

Understanding the dose-related effects is very important in reducing radiation damage in SXSS measurements. However, in many cases we need an alternative method to avoid damage, such as the addition of radical scavengers. Many of the potential scavengers described in the literature are reducing agents that neutralize the radicals (Garrison, 1987). Ethanol is usually used for stopping the radical reaction in footprinting experiments. A low concentration of DTT (a few m*M*) is most often utilized in SXSS measurements (P. Vachette, personal communication). Ascorbic acid is another candidate for preserving disulfide bonds. Since the properties of these scavengers were previously discussed thoroughly, this paper focuses on cryoprotectant agents.

In protein crystallography (O'Neill, 2001; Murray & Garman, 2002), a high concentration of glycerol [*ca* 20% (*w*/*w*)] is frequently used to reduce the level of secondary damage, that is, it intercepts the interaction of radicals in the vicinity of the protein and prevents them from reacting with the protein. Compared with the experiments carried out at temperatures close to that of liquid nitrogen, SXSS experiments are performed at room temperature, where more rapid diffusion of radicals would be expected. As described in the dose-rate effects, the dispersion conditions seem to be critical for radiation damage, and the rules from protein crystallography do not simply apply to SXSS. To evaluate the applicability of cryoprotectants to SXSS studies, three agents, glycerol, ethylene glycol and sucrose, were tested. Their molecular weights are 92, 62 and 342 Da, and their relative viscosities at 20% (*w*/*w*) are 1.734, 1.658 and 1.941, respectively. All of them contain a hydrocarbon chain with several hydroxyl side chains. These solvent additives modulate the biochemical reactions if, during the course of the reaction, there is a change in the preferential interactions of the solvent components with the reacting system.

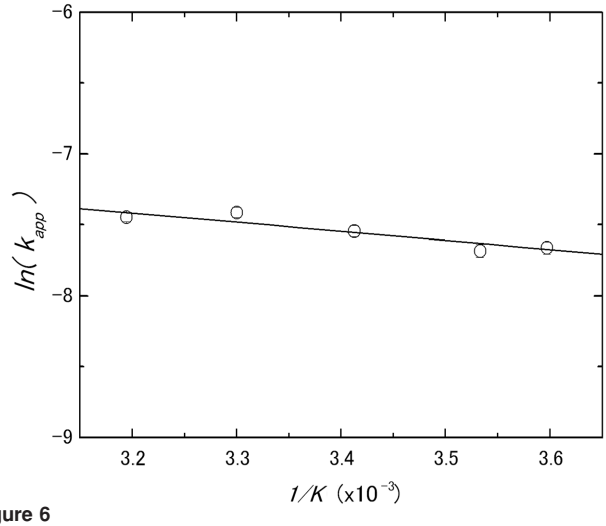

Figure 6
Arrhenius plot ($\ln k_{app}$ *versus* K^{-1}) of the radiation-induced aggregation. k_{app} was determined based on equation (7). The protein concentration was 5 mg ml^{-1} and the dose rate was 135 Gy s^{-1}. The apparent activation energy required for the radiation-induced aggregation was E_a = 1.26 ± 0.22 kcal mol^{-1}.

The SXSS results shown in Fig. 7 revealed three important findings. First, the aggregation was effectively reduced, even with a dilute concentration of the cryoprotectants (effective concentration). In the range of 0.1% (*w*/*w*) and beyond 1.0% (*w*/*w*), radiation damage was not seen in the absorbed energy of 2000 Gy (Fig. 7*a*). Second, the reduction of radiation-induced aggregation is most effective in its initial stage that is reflected by the elongation of critical dose (Fig. 7*b*). Third, the effective concentration is independent of the type of cryoprotectant (Fig. 7*c*). The effective concentration for sucrose was also 1.0% (*w*/*w*); however, it was not shown in Fig. 7(*c*) because the dose rate was one-half of that used with the other cryoprotectants. Fig. 7 suggests that only ∼1.0% (*w*/*w*) of the cryoprotectant is quite enough to reduce the radiation-induced damage to proteins in the SXSS experiments.

The first finding is crucial for understanding the suppression mechanism by the cryoprotectants. If the diffusion-control effect of solvents is important for reducing the radiation-induced aggregation, then the concentration of the cosolvents should be at least 1 *M*, *i.e. ca* 10% (*w*/*w*) (O'Neill *et al.*, 2002). The relative viscosities, the ratio of the absolute viscosity of a solution to that of water, at the effective concentration [1.0% (*w*/*w*)] are 1.020, 1.018 and 1.026 for glycerol, ethylene glycol and sucrose, respectively (*Handbook of Chemistry and Physics*, Boca Raton, Florida: CRC Press). On the other hand, 10% (*w*/*w*) of glycerol has a relative viscosity of 1.288. The Kramer theory, which assumes that the diffusion of reactants or the solvent viscosity contributes to the reaction rate (Kramers, 1940), therefore does not apply to the radical scavenging reactions by the cryoprotectants. Consequently, the reduction must be ascribed to other factors.

One possible explanation would be the change in the protein–protein interactions in the presence of a small amount of cryoprotectant. For example, Liu *et al.* (2004) recently reported a large increase in the second virial coefficient of a lysozyme solution upon the addition of glycerol or monohydric alcohols, which indicates stronger protein–protein repulsion or weaker attraction. The increase of the second virial coefficient was reported at around 10% (*w*/*w*) of gylycerol under high salt conditions (0.5 *M* NaCl) and is expected to occur with more dilute concentrations at a lower ionic strength. They interpreted these results in terms of the preferential hydration of protein (Priev *et al.*, 1996). A thicker lysozyme hydration layer in an aqueous glycerol solution can explain the glycerol-increased lysozyme–lysozyme repulsion (Liu *et al.*, 2004). This repulsive interaction consequently reduces the association of lysozyme as a result of radiation-induced aggregation. It might also reflect the elongation of critical dose.

The other factor would be the chemical properties of the hydroxyl side chains of these cryoprotectants. Hydroxyl residues are known to function as both hydrogen donors and acceptors of hydrogen bonds.

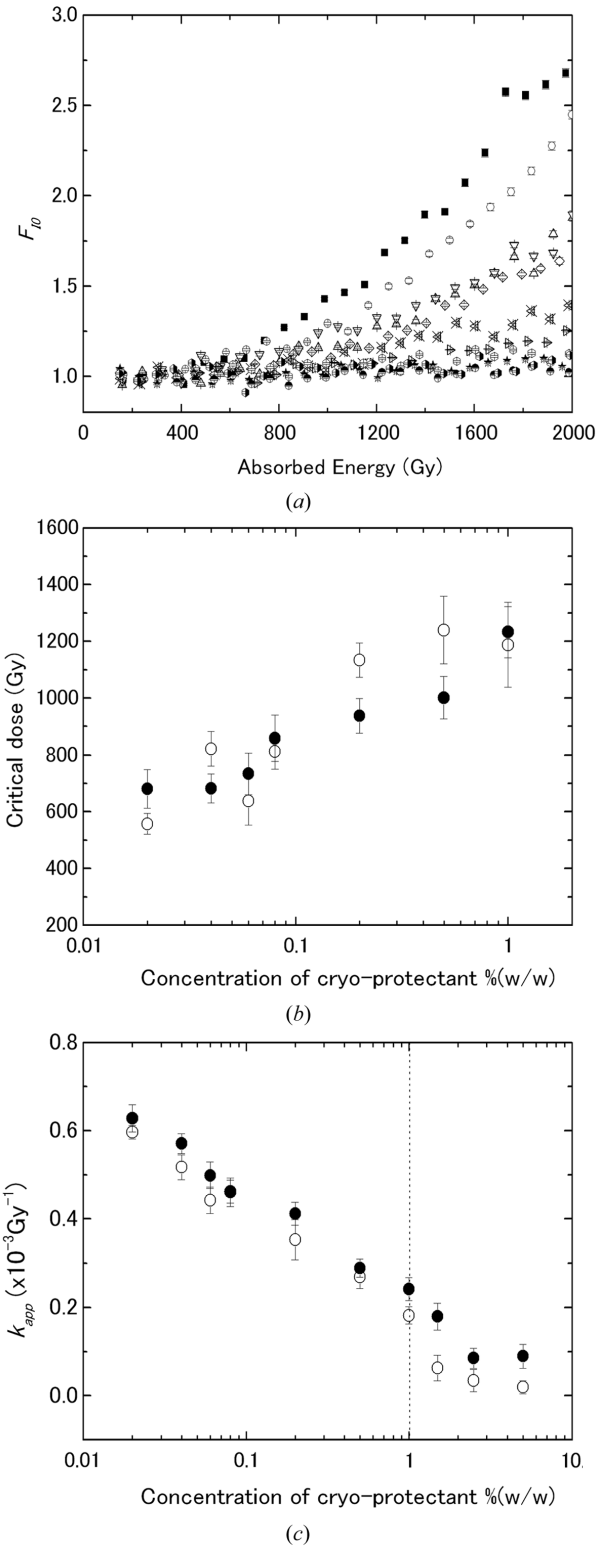

Figure 7
Effects of cryoprotectants on radiation-induced aggregation. (*a*) Dependence of the rate of increase $I(0)$ on the concentration of glycerol. Curves from the top to bottom correspond to 0, 0.02, 0.04, 0.06, 0.08, 0.2, 0.5, 1.0, 1.5, 2.5 and 5.0% (*w*/*w*). (*b*) Dependence of critical dose on the concentrations of glycerol and ethylene glycol. Open and solid circles correspond to the plots for glycerol (148 Gy s^{-1}) and ethylene glycol (148 Gy s^{-1}), respectively. The critical dose of each data point was determined based on equation (7). (*c*) The apparent rate of the aggregation corresponding to the critical dose shown in (*b*). Beyond 1.0% (broken lines), the aggregation is negligible and principally no different from each other.

The presence of hydroxyl residues could absorb the OH radicals or electrons created by X-ray radiation. The numbers of hydroxyl residues are two and three for ethylene glycol and glycerol, respectively. The contribution of the number of hydroxyl residues, however, is not conspicuous in the latter experimental findings.

The present manuscript only deals with a lysozyme solution. The reduction of radiation damage by cryoprotectants was also seen for other proteins that lack disulfide bonds (data not shown); therefore we expect that the present findings would be applicable to a wide range of SXSS measurements.

4. Concluding remarks

Radiation damage depends on the conditions of both the proteins and the probes. The apparent dose-related effects in radiation-induced aggregation observed for SXSS are therefore different from those of crystallography or radiology. This does not contradict the fact that most of the radiation damage originates from secondary chemical processes, since the radiation-induced aggregation showed a 'dilution effect' that is explained well by OH radical attacks. We propose the following process of radiation-induced aggregation: the generation of radicals in the solvent and the activation of side chains on the protein surface is followed by the association of proteins, without large conformational changes or cleavage of the polypeptide. By incorporating the present dose-related considerations, we could effectively avoid the radiation damage in SXSS experiments. It should be noted that the presence of small amounts of the cryoprotectants helped to suppress the radiation damage. Since the contribution of the viscosity is small, either the change of the protein–protein interactions or the absorption of radicals by the cryosolvents reduces the aggregation.

The authors thank Dr Yuichiro Maéda for his continuous encouragement and support for keeping the SAXS beamline at RIKEN. Mr Mitsusada Iwasa kindly helped us in the set up of the TOF-mass experiment. SA was supported by the Special Postdoctoral Researchers Program of RIKEN. This study was supported by Special Coordination Funds for Promoting Science and Technology from the Ministry of Education, Culture, Sports, Science and Technology, the Japanese Government.

References

Arai, S. & Hirai, M. (1999). *Biophys. J.* **76**, 2192–2197.
Butler, A. V., Robins, A. B. & Rotblat, J. (1960). *Proc. R. Soc.* **256**, 1.
Cherezov, V., Riedl, K. M. & Caffrey, M. (2002). *J. Synchrotron Rad.* **9**, 333–341.
Fischetti, R. F., Rodi, D. J., Mirza, A., Irving, T. C., Kondrashkina, E. & Makowski, L. (2003). *J. Synchrotron Rad.* **10**, 398–404.
Fujisawa, T., Inoko, Y. & Yagi, N. (1999). *J. Synchrotron Rad.* **6**, 1106–1114.
Fujisawa, T., Inoue, K., Oka, T., Iwamoto, H., Uruga, T., Kumasaka, T., Inoko, Y., Yagi, N., Yamamoto, M. & Ueki, T. (2000). *J. Appl. Cryst.* **33**, 797–800.
Fujisawa, T., Kostyukova, A. & Maeda, Y. (2001). *FEBS Lett.* **498**, 67–71.
Garrison, W. M. (1987). *Chem. Rev.* **87**, 381–398.
Guinier, A. & Fournet, G. (1955). *Small-Angle Scattering of X-rays.* New York: Wiley.
ICRU (1989). *Tissue Substitutes in Radiation Dosimetry and Measurement*, Report 44 of the ICRU. International Commission on Radiation Units and Measurements, Bethesda, MD, USA.
Kramers, H. A. (1940). *Physica (Utrecht)*, **7**, 284–304.
Liu, W., Bratko, D., Prausnitz, J. M. & Blanch, H. W. (2004). *Biophys. Chem.* **107**, 289–298.
Maleknia, S. D., Ralston, C. Y., Brenowitz, M. D., Downard, K. M. & Chance, M. R. (2001). *Anal. Biochem.* **289**, 103–115.
Murray, J. & Garman, E. (2002). *J. Synchrotron Rad.* **9**, 347–354.

O'Neill, P. (2001). *Studies in Physical and Theoretical Chemistry*, No. 87, *Radiation Chemistry*, edited by C. D. Jonah and B. S. M. Rao, pp. 585–622. Amsterdam: Elsevier.
O'Neill, P., Stevens, D. L. & Garman, E. F. (2002). *J. Synchrotron Rad.* **9**, 329–332.
Priev, A., Almagor, A., Yedgar, S. & Gavish, B. (1996). *Biochemistry*, **35**, 2061–2066.
Schagger, H. & von Jagow, G. (1987). *Anal. Biochem.* **166**, 368–379.
Smith, L. J., Sutcliffe, M. J., Redfield, C. & Dobson, C. M. (1993). *J. Mol. Biol.* **229**, 930–944.
Teng, T.-Y. & Moffat, K. (2000). *J. Synchrotron Rad.* **7**, 313–317.
Teng, T.-Y. & Moffat, K. (2002). *J. Synchrotron Rad.* **9**, 198–201.
Timchenko, A. A., Galzitskaya, O. V. & Serdyuk, I. N. (1997). *Proteins*, **28**, 194–201.
Weik, M., Ravelli, R. B., Kryger, G., McSweeney, S., Raves, M. L., Harel, M., Gros, P., Silman, I., Kroon, J. & Sussman, J. L. (2000). *Proc. Natl. Acad. Sci.* **97**, 623–628.
Zarzycki, J. (1987). *J. Non-Cryst. Solids*, **95/96**, 173–184.
Zimmer, K. G. (1961). *Studies on Quantitative Radiation Biology.* Edinburgh/London: Oliver & Boyd.